Revista Facultad de Ingeniería Universidad de Antioquia
ISSN: 0120-6230
revista.ingenieria@udea.edu.co
Universidad de Antioquia
Colombia

Rueda-Chacón, Hoover Fabián; Vargas-García, Cesar Augusto; Arguello-Fuentes, Henry
Single-pixel optical sensing architecture for compressive hyperspectral imaging
Revista Facultad de Ingeniería Universidad de Antioquia, núm. 73, diciembre, 2014, pp. 134-143
Universidad de Antioquia
Medellín, Colombia

Single-pixel optical sensing architecture for compressive hyperspectral imaging

Arquitectura óptica de único pixel para el sensado compresivo de imágenes hiperespectrales

Hoover Fabián Rueda-Chacón[1], Cesar Augusto Vargas-García[1], Henry Arguello-Fuentes[2]*

[1] Department of Electrical and Computer Engineering, University of Delaware. 140 Evans Hall. C.P. 19716. Newark, USA.

[2] Escuela de Ingeniería de Sistemas e Informática, Universidad Industrial de Santander. Carrera 27, Calle 9. C.P. 680002. Bucaramanga, Colombia.

(Received October 30, 2013; accepted September 24, 2014)

Abstract

Compressive hyperspectral imaging systems (CSI) capture the three-dimensional (3D) information of a scene by measuring two-dimensional (2D) coded projections in a Focal Plane Array (FPA). These projections are then exploited by means of an optimization algorithm to obtain an estimation of the underlying 3D information. The quality of the reconstructions is highly dependent on the resolution of the FPA detector, which cost grows exponentially with the resolution. High-resolution low-cost reconstructions are thus desirable. This paper proposes a Single Pixel Compressive Hyperspectral Imaging Sensor (SPHIS) to capture and reconstruct hyperspectral images. This optical architecture relies on the use of multiple snapshots of two time-varying coded apertures and a dispersive element. Several simulations with two different databases show promising results as the reliable reconstruction of a hyperspectral image can be achieved by using as few as just the 30% of its voxels.

----------*Keywords:* Single-pixel detector, hyperspectral imaging, compressive sensing, optical imaging, coded aperture-based systems

Resumen

Los sistemas de sensado de imágenes espectrales (CSI) capturan información tridimensional (3D) de una escena usando mediciones codificadas en dos dimensiones (2D). Estas mediciones son procesadas posteriormente por un algoritmo de optimización para obtener una estimación de la información

* Corresponding author: Hoover Fabián Rueda Chacón, e-mail: rueda@udel.edu

tridimensional. La calidad de las reconstrucciones obtenidas depende altamente de la resolución del detector, cuyo costo aumenta exponencialmente a mayor resolución exhiba. Así, reconstrucciones de alta resolución son requeridas, pero a bajo costo. Este artículo propone una arquitectura óptica de sensado compresivo que utiliza un único pixel como detector para la captura y reconstrucción de imágenes hiperespectrales. Esta arquitectura óptica depende del uso de múltiples capturas de imágenes procesadas por medio de dos aperturas codificadas que varían en cada toma, y un elemento de dispersión. Diferentes simulaciones con 2 bases de datos distintas muestran resultados promisorios que permiten reconstruir una imagen hiperespectral utilizando tan solo el 30% de los vóxeles de la imagen original.

----------*Palabras clave:* Detector de único pixel, imágenes hiperespectrales, sensado compresivo, sensado y procesado óptico de señales, sistemas basados en aperturas codificadas

Introduction

Hyperspectral images consist of a large amount of spatial information across a multitude of wavelengths. Traditional hyperspectral imaging sensors scan adjacent spatial zones of a scene and merge the partial results to construct a 3D spatio-spectral data cube. Pushbroom spectral imaging sensors, for instance, capture a line of spectral information of the scene per snapshot by using a dispersive element such as a prism or grating, and a Focal Plane Array (FPA) detector [1]. Therefore, the captured lines are concatenated to construct the complete spatio-spectral data cube. Hyperspectral sensors based on optical filters scan a scene by electronically tuning band-pass filters at wavelength steps such that a whole spectral region is covered [2]. Other scanning hyperspectral imaging sensors include Fabry-Pérot interferometers [3], filter patterned FPA detectors [4], integral field spectrometers [5], and whiskbroom scanners [6]. In wavelength regions of the infrared (IR) or the short wave infrared (SWIR), the cost and the dimensions of hyperspectral imaging sensors increase exponentially with the spatial resolution. For instance, the price of a 320x320 hyperspectral scanning sensor can achieve the order of hundreds of thousands of dollars [7]. Furthermore, the scanning hyperspectral sensors have the disadvantage of requiring a number of samples proportional to the dimensions of the desired data cube. More specifically, these sensors are limited by the well-known Nyquist sensing criterion [8].

Recently, the theory of Compressive Sensing (CS) [9, 10] has permitted to achieve sampling rates lower than those established by the Nyquist criterion, such that a hyperspectral signal can be sensed by using a number of samples proportional to the number of non-zero elements of the underlying signal (its sparsity). More formally, a hyperspectral signal $\mathbf{F} \in R^{M\times N\times L}$, or its vector representation $\mathbf{f} \in R^{MNL}$, is S sparse on some basis Ψ, if $\mathbf{f}=\Psi\theta$ can be approximated by a linear combination of S vectors from $\boldsymbol{\Psi}$ with $S \ll MNL$. Here, $M \times N$ represents the spatial dimensions and L is the spectral depth of the hyperspectral image. CS allows **f** to be recovered from m random projections with high probability when $m = S\log(MNL) \ll MNL$. Diverse optical architectures have been proposed to implement CS in imaging and hyperspectral imaging [1, 2, 11-13]. In order to maximally exploit the CS theory, these architectures use just a single pixel detector. The optical architectures in Compressive Spectral Imaging (CSI) area use a spectrometer as a detector, which does not completely exploit the benefits of CS. Examples of CSI sensors can be found in [14, 15].

This paper presents a new optical architecture for sensing a hyperspectral image by using a single pixel intensity detector. The sensing mechanism is based on the CS technique where the random projections are implemented by varying the random patterns of two coded apertures. More specifically, the projections in the new Single Pixel Compressive Hyperspectral Imaging Sensor (SPHIS) are given by $\mathbf{y}=\mathbf{Hf}$, where $\mathbf{H}$ represents the effect of the dispersive element and two coded apertures. The underlying data cube $\mathbf{f}$ is recovered by solving the optimization problem given by $\mathbf{f}=\Psi(\arg\min_{\theta}\|\mathbf{y}-\mathbf{H}\Psi\boldsymbol{\theta}\|_2+\tau\|\boldsymbol{\theta}\|_1)$, where τ is a regularization parameter, and $\|.\|_2$ and $\|.\|_1$ are the ℓ_2 and ℓ_1 norm operators respectively. The principal contribution of this paper lies in establishing the mathematical model of the new SPHIS architecture. Further, this paper determines the optimal transmittance of the coded apertures needed to implement the SPHIS. Several simulations illustrate the peak-signal-to-noise-ratio (PSNR) of the reconstructed data cubes as a function of the transmittance of the coded apertures and the size of the underlying data cubes. The considerable reduction in price and size of the proposed sensor makes it more suitable for diverse hyperspectral imaging applications in the IR and SWIR wavelength ranges.

Single pixel compressive hyperspectral imaging sensor (SPHIS)

The physical sensing phenomenon in the proposed system is optically realized by a couple of coded apertures, a dispersive element such as a prism, and a single pixel intensity detector as depicted in figure 1.

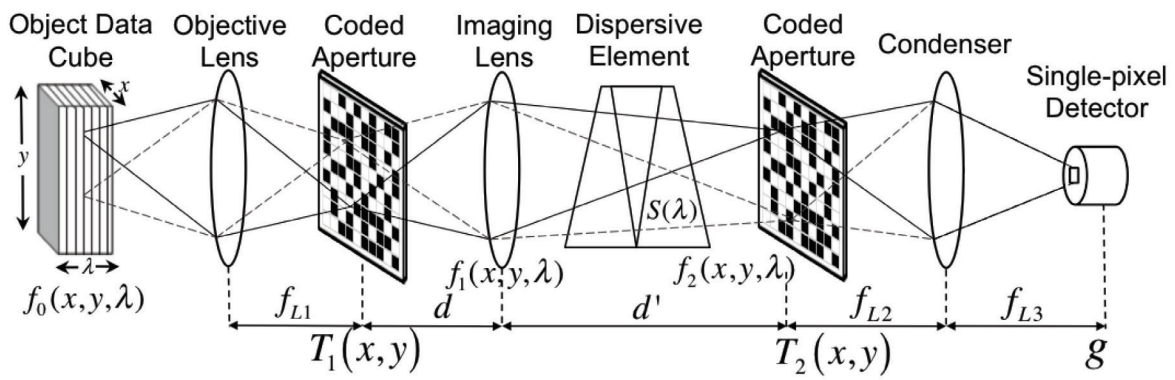

Figure 1 Optical architecture of the SPHIS. Here, f_L1, f_L2 and f_L3 represent the focal length of the lenses, whereas d and d' accounts for the image formation distance of the imaging lens

Specifically, the coding is applied to the (spatial-spectral) object data cube $f_0(x,y,\lambda)$ by means of a fixed coded aperture $T_1(x,y)$; where x and y are the spatial coordinates and λ the wavelength. The resulting coded field $f_1(x,y,\lambda)$ is subsequently modified by a dispersive element resulting on the field $f_2(x,y,\lambda)$. As the coded field $f_1(x,y,\lambda)$ traverses the prism, it is spatially sheared along one spatial axis. Hence, each coded image plane is shifted along the x axis, such that the amount of the shifts increases with the wavelength coordinate index. The field $f_2(x,y,\lambda)$ is then modified by a second coded aperture $T_2(x,y)$, and the corresponding output is then concentrated into a single pixel detector. The compressive measurements in the detector are realized by the integration of the concentrated field over the detector's spectral range sensitivity. Note that the $M\times N\times L$ voxels of the spectral data cube are condensed into a single pixel detector. SPHIS encodes the spatial information by the use of the first coded aperture, whereas the second coded aperture encodes the spectral information. Figure 2 depicts the sensing process performed by the SPHIS.

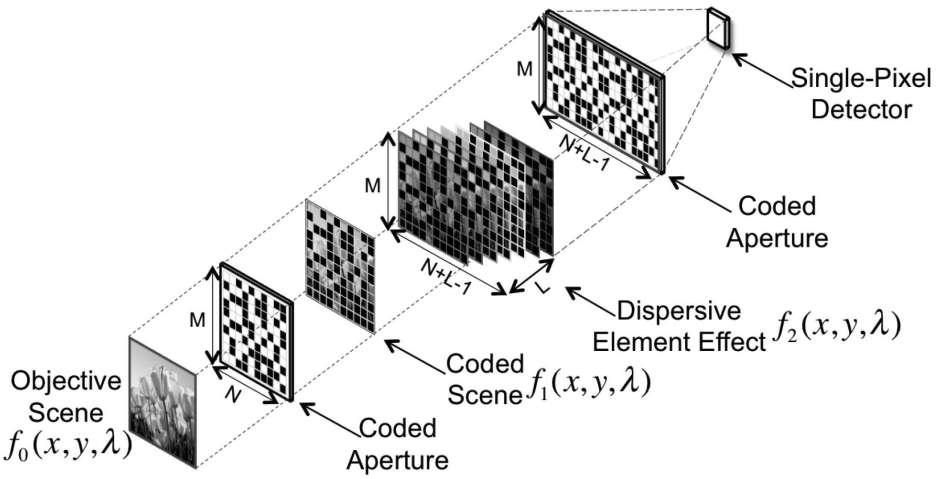

Figure 2 SPHIS sensing process. The objective scene is first coded, then dispersed and finally coded again and condensed onto a single-pixel detector

More formally, the two coded apertures used in the ℓ^{th} snapshot of the sensing process are given by eq. (1) and (2), respectively, which can be written as:

$$T_1^{\ell}(x,y) = \sum_i \sum_j (t_1^{\ell})_{ij} \,\mathrm{rect}\left(\frac{x}{\Delta} - i, \frac{y}{\Delta} - j\right) \quad (1)$$

$$T_2^{\ell}(x,y) = \sum_{i\prime} \sum_j (t_2^{\ell})_{ij} \,\mathrm{rect}\left(\frac{x}{\Delta} - i, \frac{y}{\Delta} - j\right) \quad (2)$$

where, rect() represents the rectangular step function accounting for the features shape, $(t_1^{\ell})_{ij}$ and $(t_2^{\ell})_{ij}$ represent the binary value (blocking or translucent) of the first and second coded apertures in the $(i,j)^{th}$ position, respectively, and Δ is the side size of the features in the coded apertures. Remark in eq. (1) and (2) that T_1^{ℓ} is of size $M \times N$, matching with the spatial resolution of the spectral datacube $f_0(x,y,\lambda)$, whereas T_2^{ℓ} is of size $M \times (N+L-1)$, matching with the dispersed field $f_2(x,y,\lambda)$ dimensions, as shown in figure 2. The ratio between the number of translucent and the total number of elements in a coded aperture is defined as the transmittance (or density). For instance, 30% of transmittance means that 30% of the elements in the coded aperture are translucent and the remaining are blocking. By denoting the input spectral image in discrete form as f_{ijk}, where i and j index the spatial position and k indexes the spectral band, the measurements in the SPHIS can be succinctly written as in eq. (3).

$$y_{\ell} = \sum_{i=0}^{M-1} \sum_{j=0}^{N+L-2} \left(\sum_{k=0}^{L-1} f_{i(j-k)k} \left(t_1^{\ell}\right)_{i(j-k)} \right) \left(t_2^{\ell}\right)_{ij} \quad (3)$$

where $\ell = 1,\ldots,K$ determines the ℓ^{th} single pixel measurement for a multiple-snapshot approach. Notice that the coded apertures are time-varying and change for every ℓ^{th} measurement. The single pixel measurements can be arranged into a vector $\mathbf{y} = [y_0,\ldots,y_{K-1}]^T$, which can be written as given in eq. (4) in a system of linear equations.

$$\mathbf{y} = \mathbf{Hf} = \mathbf{H\Psi_{3D}}\,\boldsymbol{\theta} = \mathbf{A\theta} \quad (4)$$

where $\mathbf{A} = \mathbf{H\Psi_{3D}} \in \mathrm{R}^{K \times MNL}$ is the sensing matrix, K is the total number of measurements, L is the number of spectral bands, and $\boldsymbol{\theta}$ is a sparse representation of the data cube in the three-dimensional basis $\mathbf{\Psi_{3D}}$. A Kronecker basis $\mathbf{\Psi_{3D}} = \mathbf{\Psi_1} \otimes \mathbf{\Psi_2} \otimes \mathbf{\Psi_3}$ is often used, where the product $\mathbf{\Psi_1} \otimes \mathbf{\Psi_2}$ is the 2D-Wavelet Symlet 8 basis and $\mathbf{\Psi_3}$ is the discrete cosine basis [16]. The matrix $\mathbf{H}$ in eq. (4) accounts for the effects of both coded apertures and the dispersive element. This matrix can be expressed as in eq. (5).

$$\mathbf{H}=\begin{bmatrix}\boldsymbol{h}_1\\ \boldsymbol{h}_2\\ \vdots\\ \boldsymbol{h}_K\end{bmatrix} \quad (5)$$

where $\boldsymbol{h}_\ell$ is particularly detailed in eq. (6), taking the form

$$\boldsymbol{h}_\ell = \boldsymbol{\mu}\mathbf{H}_2^\ell\mathbf{H}_1^\ell \quad (6)$$

such that $\boldsymbol{\mu}$ is a one-valued row vector of dimension $1\times M(N+L\text{-}1)$, $\mathbf{H}_2^\ell$ is a $M(N+L\text{-}1)\times M(N+L\text{-}1)$ matrix related to the second coded aperture in which its diagonal accounts for the values of T_2^ℓ, and $\mathbf{H}_1^\ell$ is a $M(N+L\text{-}1)\times MNL$ matrix related to the first coded aperture T_1^ℓ and the dispersive element. For simulations, the entries of both coded apertures are considered binary and change for every snapshot ℓ, and the dispersive element exhibits a linear dispersion behavior. In practice, however, it is necessary to take into account the various optical artifacts and non-idealities of the optical system [17]. The recovery of the underlying hyperspectral signal in the SPHIS entails solving an underdetermined linear system of equations stated in eq. (7). Given the set of measurements $\mathbf{y}$, the inverse compressive sensing problem consists on recovering $\mathbf{f}$ such that the ℓ_1-ℓ_2 cost function is minimized as

$$\hat{\mathbf{f}} = \boldsymbol{\Psi}_{\mathbf{3D}}(\text{argmin}_{\boldsymbol{\theta}}\|\mathbf{y} - \mathbf{A}\boldsymbol{\theta}\|_2^2 + \tau\|\boldsymbol{\theta}\|_1) \quad (7)$$

where τ is a regularization constant. Notice that the sensing matrix $\mathbf{A}$ plays a pivotal role and thus its design is critical in this imaging problem [18, 19].

Simulations and results

To test the SPHIS system developed in this paper, two hyperspectral data cubes $\mathbf{F}$ which serve as the input images of the system were first captured in the laboratory using a wide-band Xenon lamp as the light source, a visible monochromator which spans the spectral range between 450 and 650 nanometers, and a CCD camera exhibiting a pixel pitch of 9.9 micrometers. These data cubes exhibit either 64×64 or 128×128 pixels of spatial resolution, and both of them L=8 spectral bands (Figure 3). The entries of the time-varying coded apertures presented in eq. (1) and (2) are realizations of a Bernoulli random variable with parameter p set as 0.1 (10%), 0.25 (25%) and 0.5 (50%), representing the total transmittance (Tr) or translucent elements of the codes. The dispersive element is a double-amici prism exhibiting linear dispersion [20], and the detector is a single pixel which integrates the intensity focused by the condenser. The compressive sensing-based reconstruction GPSR algorithm [21] is employed to solve the optimization problem in eq. (7) and optimized to admit large amounts of data. The basis representation $\boldsymbol{\Psi}_{\mathbf{3D}}$ is set to be the Kronecker product as stated in eq. (4). All simulations were conducted and timed on the same workstation with an Intel Core i7 processor (8 cores at 3.40 GHz), 32 GB of memory (DDR3 at 1067 MHz), running Windows 7 Enterprise Edition and Matlab R2012a. The quality of the reconstructions is measured through the peak-signal-to-noise-ratio (PSNR) evaluated per each band, and defined in eq. (8) as,

$$PSNR_k = 10\log_{10}\left(\frac{\max(F_k^2)}{\frac{1}{MN}\sum_{i=0}^{M-1}\sum_{j=0}^{N-1}\left[F_k^2(i,j)-\hat{F}_k^2(i,j)\right]}\right) \quad (8)$$

where F_k represents the k^{th} original band and $\hat{F}_k$ is the k^{th} reconstructed band.

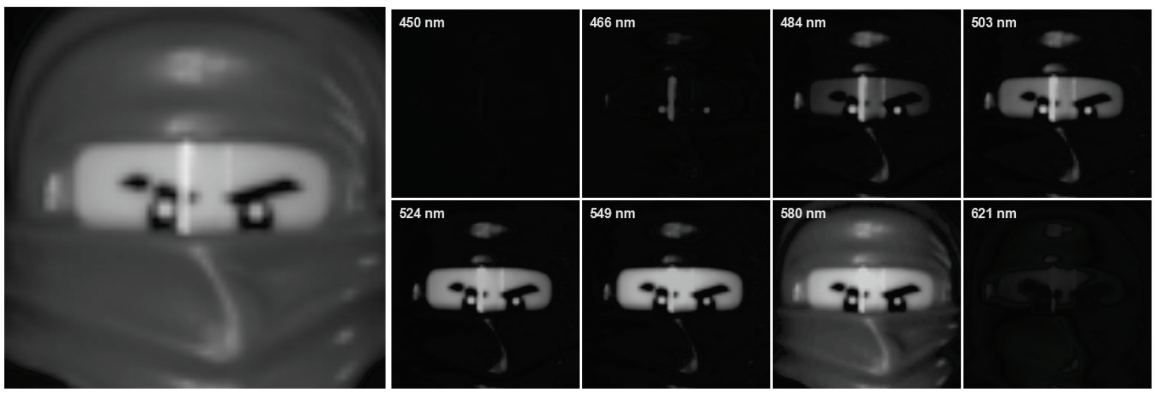

(a) Spectral data cube exhibiting 64×64×8 voxels

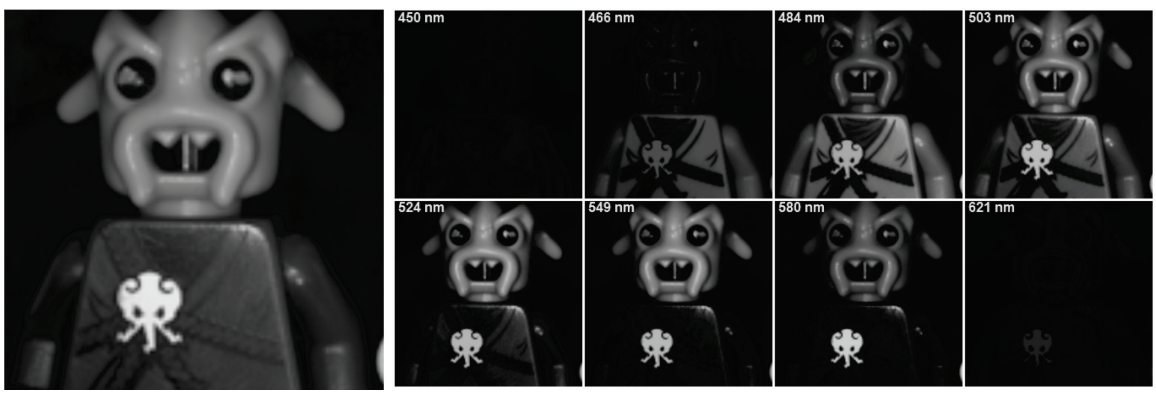

(b) Spectral data cube exhibiting 128×128×8 voxels

Figure 3 Spectral data cubes used for simulations

Figure 4 shows the PSNR behavior as well as the reconstruction results mapped to an RGB profile for different transmittance/snapshot configurations. The number of snapshots K is indicated as a percentage of the total size of the source datacube. Thus, 10% of snapshots for the smaller data cube refer to $0.1*(64*64*8)\simeq 3277$ snapshots, whereas for the larger data cube refers to $0.1*(128*128*8)\simeq 13107$ snapshots. This percentage representation of the snapshots permits to analyze the amount of information required to reconstruct the data cube. Notice that higher PSNR values are attained using greater number of snapshots, reaching the Nyquist criterion when 100% of snapshots are used. The results in figure 4 vary the amount of snapshots between 10% and 50%.

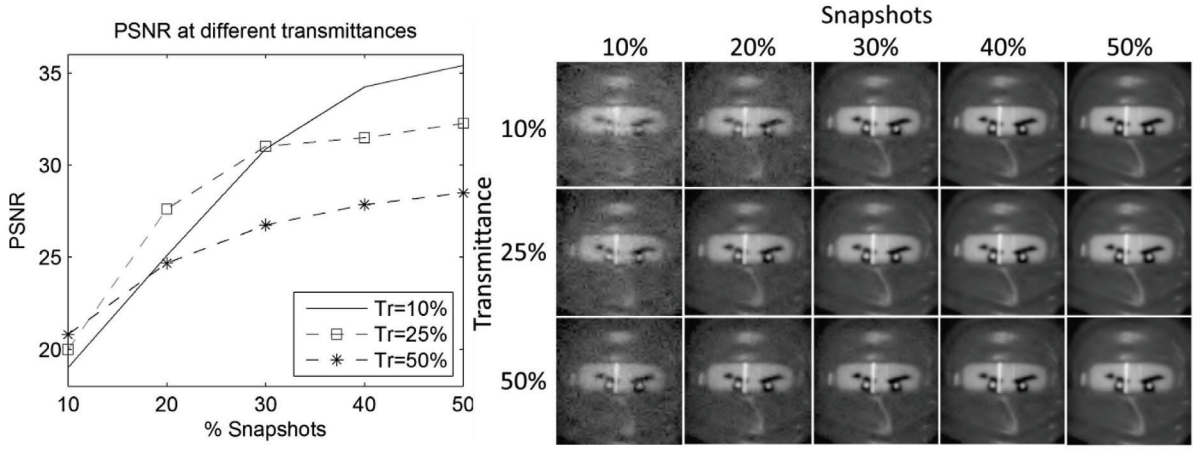

(a) Reconstruction results for the 64×64×8 spectral data cube

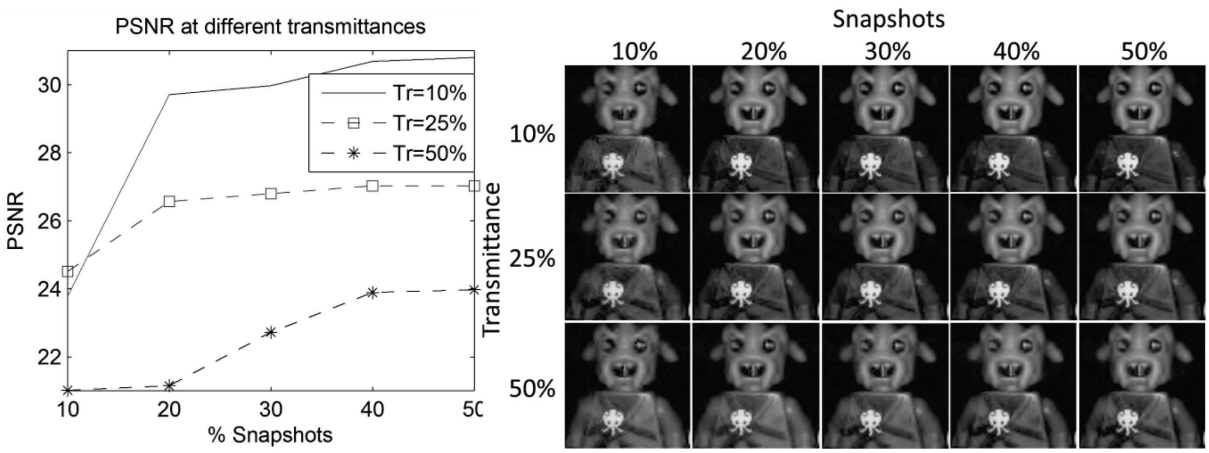

(b) Reconstruction results for the 128×128×8 spectral data cube

Figure 4 Reconstruction PSNR comparison varying the number of snapshots between 10% to 50% and the transmittance (Tr) levels between 10%, 25% and 50%. Notice that these pictures are RGB representations of the reconstructed data cubes.

Results show that there exists a trade-off between the number of single pixel measurements and the transmittance (Tr) of the corresponding coded apertures used in the sensing process. For instance, results in figure 4 show that greater spatial PSNR values are achieved with lower transmittance percentages as the number of captured snapshots grows. Figure 5 depicts the full spectral data cubes reconstructions achieved with the best transmittance (10%), comparing the results obtained using 10% and 50% of snapshots. These results indicate the improvement achieved along the whole range of wavelengths.

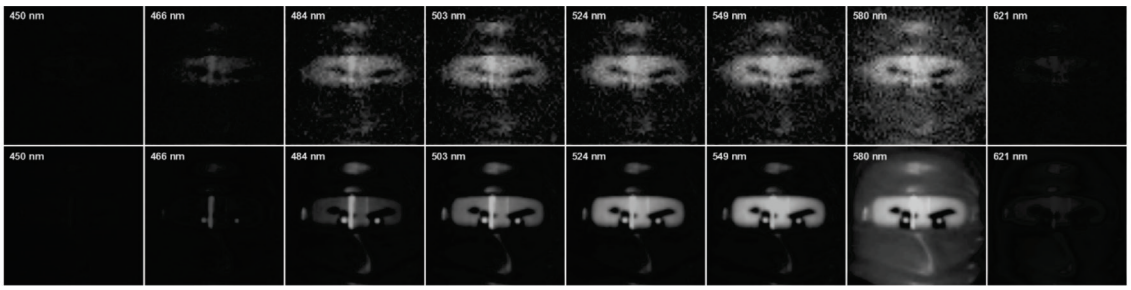

(a) 64×64×8 reconstruction using (1st row) 10% of shots and (2nd row) 50% shots

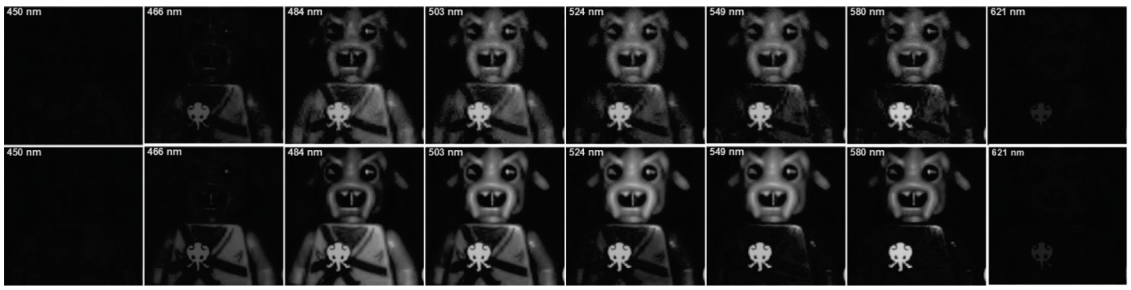

(b) 128×128×8 reconstruction using (1st row) 10% of shots and (2nd row) 50% shots

Figure 5 Reconstructed spectral data cubes when capturing 10% and 50% of snapshots, fixing the transmittance to 10%

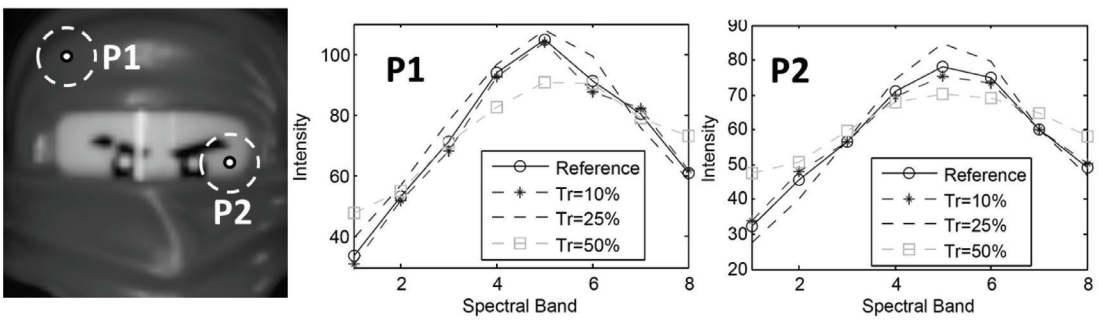

(a) Spectral signatures for the 64×64×8 spectral data cube

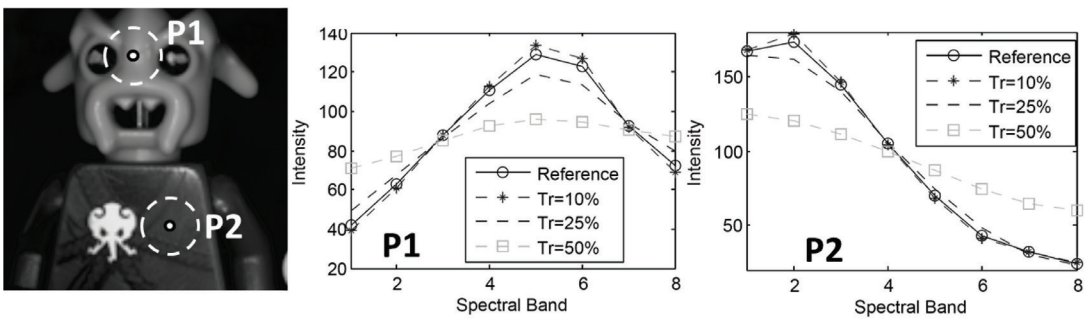

(b) Spectral signatures for the 128×128×8 spectral data cube

Figure 6 Spectral signatures comparison when using 30% of snapshots and different transmittance levels for both spectral data cubes. The spectral signatures are presented for the spatial locations indicated by the points P1 and P2 in the figures

The spectral quality of the reconstructed data cubes was also analyzed, by picking 2 points from the scene and plotting their corresponding spectral signatures. Figure 6 shows the spectral signatures of the original data cubes compared with the corresponding reconstructions obtained for different levels of transmittance using 30% of snapshots. Notice that the reconstructed spectral signatures get closer to the original as the transmittance decreases, being approximately similar the ones with 10% and 25%. Thus, good reconstruction results can be achieved by using just 30% of the original data when the coded apertures exhibit 10% of transmittance.

Conclusions

The optical design and matrix model of a Single Pixel Compressive Hyperspectral Imaging Sensor (SPHIS) have been presented. Simulations show promising results as the reconstruction of a hyperspectral image can be achieved by using just the 30% of the number of samples required by the Nyquist criterion. The spectral data cubes can be reconstructed exhibiting mean PSNR values up to 30 dB. Spectral signatures comparison confirms the outstanding quality of the reconstructions, thus leading towards low-cost, low-complexity compressive hyperspectral imaging sensors. Despite the paper focuses on spectral images lying on the visible electromagnetic spectrum, the proposed idea along with the optical design can be easily extrapolated to operate on the infrared electromagnetic spectrum where the cost of the sensors increase as higher resolution they exhibit.

Acknowledgments

This research was supported in part by Fulbright and COLCIENCIAS, and by the Vicerrectoría de Investigación y Extension from the Universidad Industrial de Santander (VIE-UIS) under the grants 1363 and 1368.

References

1. W. Chan, K. Charan, D. Takhar, K. Kelly, R. Baraniuk, D. Mittleman. “A single-pixel terahertz imaging system based on compressed sensing”. *Applied Physics Letters*. Vol. 93. 2008. pp. 121105-121105-3.

2. M. Duarte, M. Davenport, D. Takhar, J. Laska, T. Sun, K. Kelly, R. Baraniuk. “Single-Pixel Imaging via Compressive Sampling”. *IEEE Signal Processing Magazine*. Vol. 25. 2008. pp. 83–91.

3. D. Hays, A. Zribi, S. Chandrasekaran, S. Goravar, S. Maity, L. Douglas, K. Hsu, A. Banerjee. “A hybrid mems–fiber optic tunable fabry–perot filter”. *IEEE Journal of Microelectromechanical Systems.* Vol. 19. 2010. pp. 419 – 429.

4. J. Brauers, T. Aach. *A color filter array based multispectral camera*. Proceedings of the 12 Workshop Farbbildverarbeitung, October 5-6. Ilmenau, Germany. 2006.

5. C. Vanderriest. “Integral field spectroscopy with optical fibers”. *3D Optical Spectroscopic Methods in Astronomy, G. Comte and M. Marcelin, eds Astron. Soc. Pac*. Vol. 71. 1995. pp. 209-218.

6. R. Green, M. Eastwood, C. Sarture, T. Chrien, M. Aronsson, B. Chippendale, et al. “Imaging spectroscopy and the airborne visible/ infrared imaging spectrometer (AVIRIS)”. *Rem. Sens. Environ.* Vol. 65. 1998. pp. 227-248.

7. R. Willett, R. Marcia, J. Nichols. “Compressed sensing for practical optical systems: a tutorial”. *Optical Engineering*. Vol. 50. 2011. pp. 072601 1-13.

8. H. Nyquist. “Certain topics in telegraph transmission theory”. *IEEE Trans.* Vol. 47. 1928. pp. 617-644.

9. E. Candès, J. Romberg, T. Tao. “Robust uncertainty principles: Exact signal reconstruction from highly incomplete frequency information”. *IEEE Transactions on Information Theory*. Vol. 52. 2006. pp. 489–509.

10. D. Donoho. “Compressed sensing”. *IEEE Transactions on Information Theory.* Vol. 52. 2006. pp. 1289–1306.

11. V. Durán, P. Clemente, M. Fernández-Alonso, E. Tajahuerce, J. Lancis. “Single-pixel polarimetric imaging”. *Optics Letters.* Vol. 37. 2012. pp. 824–826.

12. F. Magalhães, M. Abolbashari, F. Raújo, M. Correia, F. Farahi. “High-resolution hyperspectral single-pixel imaging system based on compressive sensing”. *Optical Engineering.* Vol. 51. 2012. pp. 1–6.

13. Y. August, C. Vachman, Y. Rivenson, A. Stern. “Compressive hyperspectral imaging by random separable projections in both the spatial and the spectral domains”. *Applied Optics.* Vol. 52. 2013. pp. D46-D54.

14. H. Rueda, H. Arguello. "Spatial super-resolution in coded aperture-based optical compressive hyperspectral imaging systems". *Revista Facultad de Ingeniería Universidad de Antioquia*. Vol. 67. 2013. pp. 7-18.

15. A. Wagadarikar, R. John, R. Willett, D. Brady. "Single disperser design for coded aperture snapshot spectral imager". *Applied Optics.* Vol. 47. 2008. pp. B44-B51.

16. H. Arguello, G. Arce. "Rank Minimization Code Aperture Design for Spectrally Selective Compressive Imaging". *IEEE Transactions on Image Processing.* Vol. 22. 2013. pp. 941-954.

17. H. Arguello, H. Rueda, Y. Wu, D. Prather, G. Arce. "Higher-order computational model for coded aperture spectral imaging". *Applied Optics*. Vol. 52. 2013. pp. D12-D21.

18. H. Arguello, C. Correa, G. Arce. "Fast lapped block reconstructions in compressive spectral imaging". *Applied Optics*. Vol. 52. 2013. pp. D32-D45.

19. H. Arguello, G. Arce. "Code aperture optimization for spectrally agile compressive imaging". *J. Opt. Soc. Am. A.* Vol. 28. 2011. pp. 2400-2413.

20. Y. Wu, I. Mirza, P. Ye, G. Arce, D. Prather. *Development of a DMD-based compressive sampling hyperspectral imaging (CS-HSI) system*. Proceedings of the SPIE 7932, Emerging Digital Micro-mirror Device Based Systems and Applications III, 79320I. San Francisco, USA. 2011.

21. M. Figueiredo, R. Nowak, S. Wright. "Gradient projection for sparse reconstruction: Application to compressed sensing and other inverse problems". *IEEE Journal of Selected Topics in Signal Processing*. Vol. 1. 2007. pp. 586–597.